AIP Journal of Applied Physics

Enhanced magnetoimpedance and field sensitivity in microstructure controlled FeSiCuNbB ribbons

Trilochan Sahoo, Amaresh Chandra Mishra, V. Srinivas, T. K. Nath, M. Srinivas, and B. Majumdar

Citation: Journal of Applied Physics **110**, 083918 (2011); doi: 10.1063/1.3656450
View online: http://dx.doi.org/10.1063/1.3656450
View Table of Contents: http://scitation.aip.org/content/aip/journal/jap/110/8?ver=pdfcov
Published by the AIP Publishing

Enhanced magnetoimpedance and field sensitivity in microstructure controlled FeSiCuNbB ribbons

Trilochan Sahoo,[1] Amaresh Chandra Mishra,[1] V. Srinivas,[1,3,a)] T. K. Nath,[1] M. Srinivas,[2] and B. Majumdar[2]
[1]*Department of Physics and Meteorology, Indian Institute of Technology Kharagpur, Kharagpur 721 302, India*
[2]*Advanced Magnetics Group, Defence Metallurgical Research Laboratory, Hyderabad 500 058, India*
[3]*Department of Physics, Indian Institute of Technology Madras, Chennai 600 036, India*

(Received 29 July 2011; accepted 15 September 2011; published online 28 October 2011)

$Fe_{73.5}Si_{13.5}Cu_1Nb_3B_9$ and $Fe_{77.2}Si_{11.2}Cu_{0.8}Nb_{3.3}B_{7.5}$ nanocomposite materials consisting of nanocrystalline phase in an amorphous matrix were obtained by heat-treatment of their precursor amorphous ribbons. The influence of structural modifications induced during the heat-treatment on soft magnetic properties and magnetoimpedance (MI) effect have been studied. The structural investigations on both these ribbons revealed the presence of two phases, fine grained Fe_3Si phase and a residual amorphous phase on heat-treatment. The maximum MI ratio obtained in the present study is 95% at $f = 4$ MHz, for the optimized heat-treated $Fe_{77.2}Si_{11.2}Cu_{0.8}Nb_{3.3}B_{7.5}$ ribbon. This is ascribed to the increase in magnetic permeability and decrease in coercive force and intrinsic resistivity. Moreover, a maximum magnetic field sensitivity (ξ) of 8.3%/Oe at $f = 2.5$ MHz is obtained, for the optimized nanocrystalline $Fe_{73.5}Si_{13.5}Cu_1Nb_3B_9$ ribbon. This suggests that tailoring of the nanocrystalline microstructures induced by optimum heat-treatment conditions can result in obtaining excellent combinations of the magnetic permeability and resistivity. Our results indicate that these Fe-based nanocrystalline materials can be ideally used for low magnetic field and high frequency sensor applications. © *2011 American Institute of Physics*. [doi:10.1063/1.3656450]

I. INTRODUCTION

Nanocrystalline FeSiCuNbB alloys, popularly known as FINEMET, are the subject of recent research interest because of their excellent combination of soft magnetic properties, i.e., very high permeability, low coercive force, and nearly zero value of magnetostriction (λ). This can be achieved upon suitable partial nanocrystallization of amorphous phase into α-Fe(Si) and/or Fe_3Si phase (with a mean grain size ≈ 10 nm).[1] These alloys in amorphous state are produced by rapid solidification technique. The nanocrystallization is done through controlled devitrification of amorphous ribbons.[2] The improvement of the soft magnetic properties of metallic alloys mainly depends on the proper selection of the main alloy composition and development of the appropriate microstructure through suitable heat-treatment conditions.[3] These soft magnetic alloys also find applications as magnetic heads and sensors based on the magnetoimpedance (MI) effects.[4,5] The MI effect is a classical electromagnetic phenomenon, where the impedance of a ferromagnetic conductor changes significantly under the application of a longitudinal dc magnetic field. The electromagnetic origin of the MI effect has been attributed to the combination of skin effect and the field dependence of circumferential/transverse magnetic permeability (μ_t') associated with the circular/transverse motion of magnetic moments.[6] At a given frequency, the application of a dc magnetic field (H_{dc}) changes μ_t' and hence the magnetic penetration depth, δ_m. Therefore, the MI effect can be achieved in magnetic materials where μ_t' is high and ρ is small. In this respect, Co-based amorphous alloys (in the form of ribbons/wires) have been found to exhibit large MI effect due to their large transverse magnetic permeability and are potential candidates for MI sensor applications.[7–9] However, one disadvantage of Co-based materials is their high resisitivity. Since Fe-based nanocrystalline materials have low resistivity as compared to Co-based amorphous alloys, they are expected to show larger MI values.

It is now well established that in a two-phase nanocrystalline FeSiCuNbB alloy system, the extremely soft magnetic behavior is a consequence of the reduced grain size D of α-Fe(Si) or Fe_3Si microstructures.[1] When these structural changes occur on a scale smaller than the magnetic exchange correlation length $L_0 = (A/K)^{1/2}$, the magnetization cannot follow the local anisotropy axis and stay essentially homogeneous within L_0 due to the smoothing effect of the exchange interaction energy, A. Thus, the effective anisotropy of the randomly oriented grains is largely averaged out, and the material becomes soft magnetic for $D < L_0$ ($L_0 \approx 5-10$ nm for Co-based to about 20–40 nm for Fe-based alloys). As a result of that, the effective anisotropy is reduced three orders of magnitude at the macroscopic level.[10] Furthermore, magnetic anisotropy in some amorphous alloys is dominated by magnetostrictive phenomena. But, in the case of nanocrystalline FINEMET type of alloys, the resultant magnetoelastic anisotropy is very small, because there is a compensation between negative magnetostriction of the nanocrystalline α-Fe(Si) phase ($\lambda_{nc} \approx -6 \times 10^{-6}$) and positive magnetostriction of the amorphous interface ($\lambda_{amorph} \approx 20 \times 10^{-6}$).[11,12] This suggests

a)Author to whom correspondence should be addressed. Electronic mail: veeturi@iitm.ac.in.

that the magnetostriction value can be nullified through optimum heat-treatment. Therefore, the exact composition of these phases, the amount of each of them, the grain size and other parameters need to be monitored during partial crystallization, in order to obtain best performance of the final product. In our earlier works,[13,14] we have shown that the structural modifications in FeSiCuNbB ribbons induced during heat-treatment significantly improve the magnetic properties and MI response.

In this report, our efforts have been devoted to investigate the microstructures in $Fe_{73.5}Si_{13.5}Cu_1Nb_3B_9$ and $Fe_{77.2}Si_{11.2}Cu_{0.8}Nb_{3.3}B_{7.5}$ ribbons in their as-quenched state and heat-treated at different temperatures that affect the magnetic properties and MI behavior of the alloys. In particular, our objective is to find an optimal heat-treatment condition not only for high magnetic softness but also to make the alloy more promising for high frequency and low magnetic field sensors by getting the best MI response. Our present results show the soft magnetic properties are pronounced in $Fe_{77.2}Si_{11.2}Cu_{0.8}Nb_{3.3}B_{7.5}$ compared to $Fe_{73.5}Si_{13.5}Cu_1Nb_3B_9$ alloy ribbons and hence the MI response.

II. EXPERIMENTAL DETAILS

Amorphous Fe-based ribbons with nominal composition $Fe_{73.5}Si_{13.5}Cu_1Nb_3B_9$ and $Fe_{77.2}Si_{11.2}Cu_{0.8}Nb_{3.3}B_{7.5}$ (hereafter referred to as ***FIN-1*** and ***FIN-2***, respectively) were prepared by melting pure Fe, Si, Cu, Nb, and B elements in a vacuum induction-melting furnace. Ribbons of 25 μm thick and 1 mm width were obtained by the melt-spinning technique at a wheel speed of 47 m/s in a controlled argon atmosphere. The amorphous nature of the samples was confirmed through X-ray diffraction (XRD) study. The crystallization temperature of these ribbons was determined using a differential scanning calorimeter (DSC) (TA Instruments-DSC 910S) at a scanning rate of 20 °C/min. As-quenched ribbons were heat-treated at selected temperatures of 500, 525, 550, 575, 600, and 625 °C for 30 min in a vacuum furnace. The crystallization process of the heat-treated ribbons was monitored using X-ray diffractometer (Philips PW 1710) with Co-K_α ($\lambda = 0.17889$ nm) radiation, and the surface topography in nanoscale of the as-quenched and heat-treated samples was investigated using a 5 kV field emission scanning electron microscope (FESEM) (Carl Zeiss, Supra 40). A coercimeter (FÖSTER-KOERZIMET 1.095) was used to determine the coercivity of the samples, while the dc resistivity measurements were performed using a four-terminal contact method. Impedance and permeability measurements were performed by impedance analyzer (Agilent 4294A) using 42941A standard probe on 50 mm long ribbons placed in the homogeneous magnetic field produced through a home-made Helmholtz coil in a frequency range of 0.5–20 MHz. The applied ac current flowing across the sample was kept constant at 10 mA. The external dc magnetic field, $\boldsymbol{H_{dc}}$, was generated by the Helmholtz coil with an axis perpendicular to the Earth's magnetic field to allow field variation of $-76 \leq \boldsymbol{H_{dc}} \leq 76$ Oe. The percentage change of magnetoimpedance (i.e., MI ratio) with applied magnetic field has been expressed as

$$MI = \left(\frac{\Delta Z}{Z}\right)(\%) = \left(\frac{Z(H_{dc}) - Z(H_{\max})}{Z(H_{\max})}\right) \times 100, \quad (1)$$

where $\boldsymbol{H_{max}} = 76$ Oe, the maximum applied field. Real and imaginary parts of the complex permeability, $\boldsymbol{\mu^* = \mu'(f) - \mu''(f)}$, was measured by placing the ribbon in a small rectangular pick-up coil, and the oscillating current through the pick-up coil was maintained constant at 10 mA.

III. RESULTS AND DISCUSSIONS

A. Microstructural analysis

Figures 1(i) and 1(ii) show the X-ray diffraction patterns from the free surface of the as-quenched and heat-treated ***FIN-1*** and ***FIN-2*** ribbons, respectively. It is observed that as-quenched ribbons are fully amorphous as confirmed through the presence of a broad halo obtained nearly at $2\theta = 53°$. On heat-treatment of these samples at temperatures above 525 °C, three diffraction peaks have been observed in XRD patterns and identified as Fe_3Si phase with representative peaks (2 2 0), (4 0 0), and (4 2 2). The mean crystallite size ($\boldsymbol{D_1}$) of the Fe_3Si phase at different heat-treatment temperatures ($\boldsymbol{T_a}$) was estimated using Scherrer's equation from the full width at half maxima (FWHM) of the (2 2 0) diffraction peak, and the variation of $\boldsymbol{D_1}$ with $\boldsymbol{T_a}$ is shown in Fig. 2. It is observed that the crystallite size marginally increases from 10 nm to 12 nm in the case of ***FIN-2*** as the $\boldsymbol{T_a}$ is raised from 525 °C to 625 °C, whereas for ***FIN-1*** alloy, the

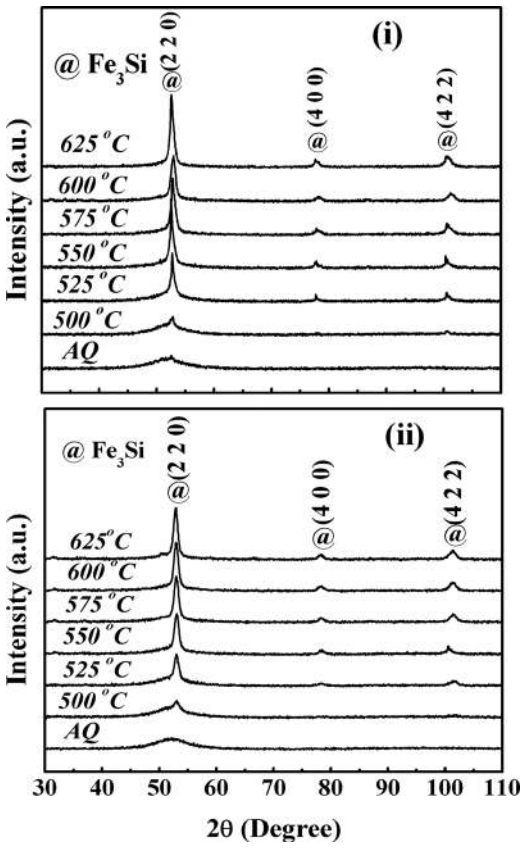

FIG. 1 X-ray diffraction pattern of as-quenched and heat-treated ***(i) FIN-1*** and ***(ii) FIN-2*** ribbons.

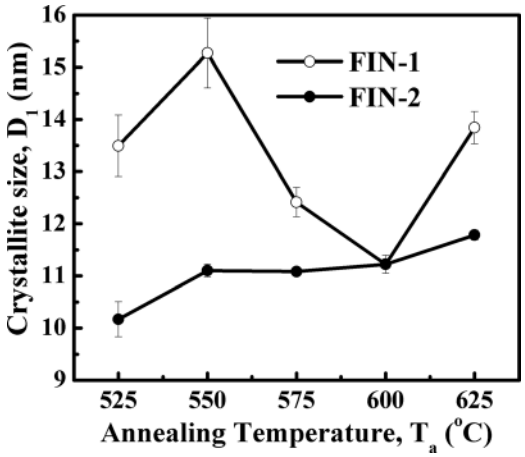

FIG. 2. Crystallite size (D_1) of as-quenched and heat-treated ***FIN-1*** and ***FIN-2*** ribbons.

variation of crystallite size with T_a appears to be more dramatic. The D_1 initially increases from 13.5 to 15.5 nm at 550 °C, decreases to 11 nm at 600 °C, and then again increases to 14 nm with T_a.

Surface micrographs of as-quenched and heat-treated ribbons of ***FIN-1*** and ***FIN-2*** alloys are shown in Figs. 3 and 4, respectively. As-quenched ribbons exhibit featureless uniform background indicating the absence of crystalline phases, while the heat-treated ribbons show the presence of nanocrystalline microstructures embedded in the amorphous matrix. With the increase in T_a, both number and size of the grains increase. These changes in microstructures are strongly reflected in their electrical and magnetic properties.

B. Electrical and magnetic properties

Figures 5(i) and 5(ii) show dc resistivity (ρ) and coercivity (H_c) as a function of heat-treatment temperature (T_a) for both the ribbons, respectively. It can be observed that ρ decreases slowly from the as-quenched (i.e., amorphous) state to the ribbon heat-treated at 500 °C, which can be attributed to the surface crystallization of the ribbons confirmed through FESEM studies. No significant changes are seen in the data obtained through X-ray diffraction studies on bulk ribbons. With further increase in the T_a (i.e., beyond 500 °C), a monotonous decrease in the ρ value is observed, which is a consequence of observable change in the crystallization (i.e., nucleation of Fe_3Si phase) obtained through X-ray diffraction studies. This strong (~20%) reduction in the resistivity of the nanocrystalline ribbons reduces the magnetic penetration depth at higher frequencies, which contributes to increasing the impedance of the samples. Moreover, the higher ρ value of ***FIN-1*** over ***FIN-2*** alloy in the entire range of T_a can be ascribed as a higher percentage of Silicon in the amorphous matrix of ***FIN-1*** than ***FIN-2*** ribbon.

The T_a dependence of H_c indicates that for ***FIN-1***, H_c value increases first from 1.6 Oe in the as-quenched state to 2.6 Oe in the heat-treated state of 500 °C. With further increment in T_a, H_c value decreases to 0.7 Oe in the heat-treated state of 575 °C and then abruptly increases to around 18 Oe in the heat-treated state of 625 °C. On the other hand, for

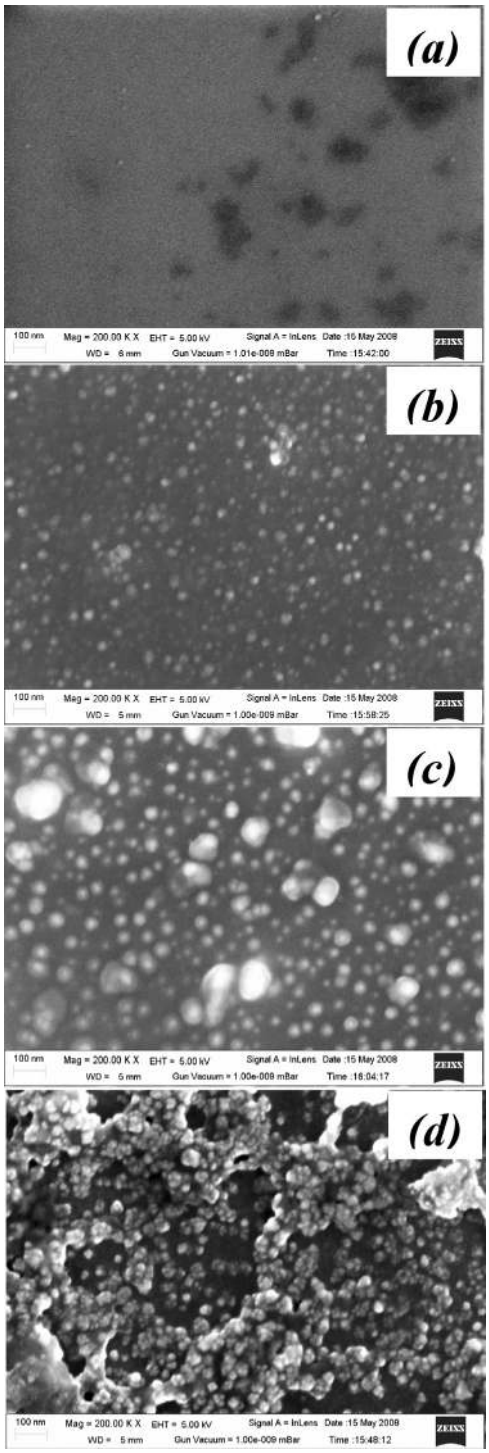

FIG. 3. FESEM micrographs of *(a)* as-quenched, *(b)* 550 °C, *(c)* 575 °C, and *(d)* 600 °C heat-treated ***FIN-1*** ribbons.

FIN-2, H_c value decreases from about 0.21 Oe in the as-quenched state to 0.04 Oe at the higher heat-treatment temperature of 575 °C and then increases to a great extent 1.67 Oe for the sample heat-treated at 625 °C. A similar T_a dependence of H_c has been reported in earlier reports.[15,16] The obtained coercivity (H_c) of ***FIN-1*** sample in the heat-treated state of 500 °C is greater than the as-quenched state, which is a consequence of stress relaxation induced earlier during the rapid solidification technique. The decrease in H_c value for $T_a > 500$ °C of both these alloys can be attributed

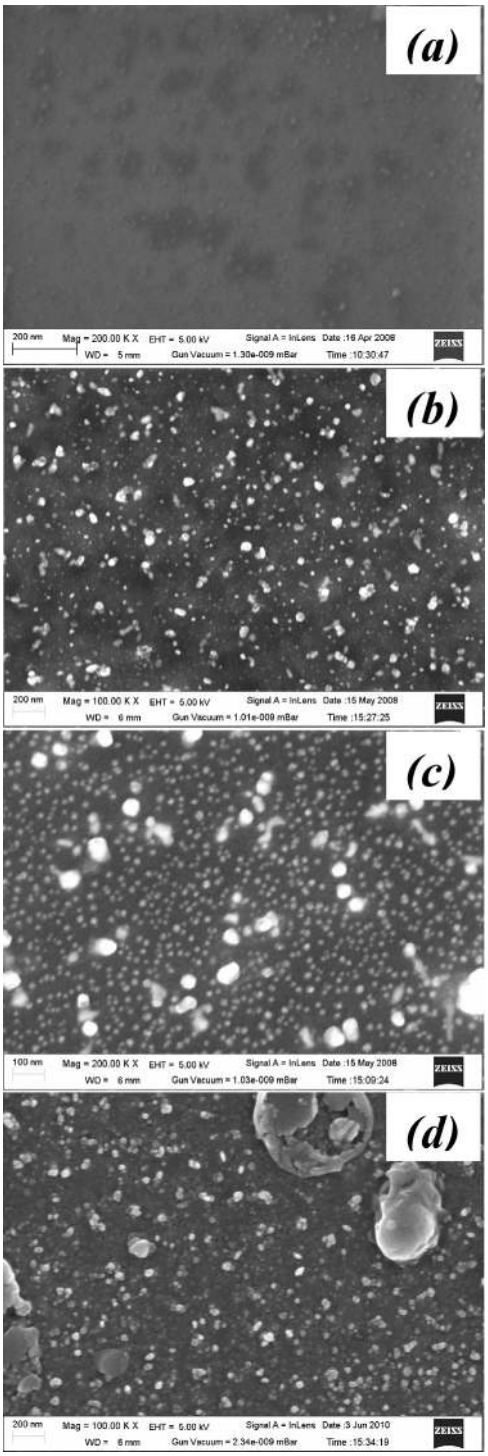

FIG. 4. FESEM micrographs of ***(a)*** as-quenched, ***(b)*** 550 °C, ***(c)*** 575 °C, and ***(d)*** 600 °C heat-treated ***FIN-2*** ribbons.

to the nucleation of soft magnetic Fe_3Si phase. The minimum H_c value occurs for the samples heat-treated at 575 °C indicating optimum crystallization of Fe_3Si phase. With further increment in T_a, the value increases; this might be due to the nucleation of hard magnetic (i.e., Fe_3B or, Fe_2B) phases and significant decrease in volume fraction of the amorphous matrix through which the nanocrystalline grains are coupled. In our earlier X-ray diffraction patterns, these phases are not found in the discussed T_a range, which might be due to very low intensity of these phases below the sensitivity of X-ray diffractometer. The superfine Fe_3Si nanocrystallites of ***FIN-2*** over ***FIN-1*** ribbon depict lower H_c values in the entire heat-treatment range.

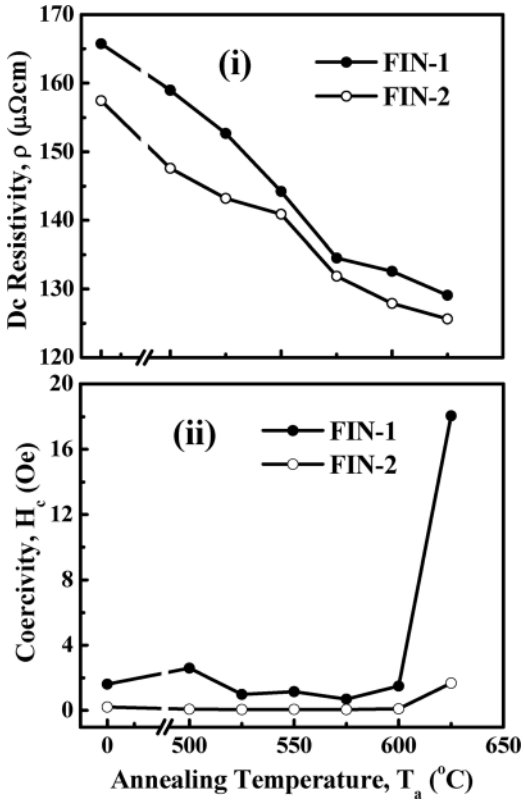

FIG. 5. Heat-treatment temperature ***(T_a)*** dependence of ***(i)*** dc resistivity ***(ρ)*** and ***(ii)*** coercivity ***(H_c)*** of ***FIN-1*** and ***FIN-2*** ribbons.

C. Ac magnetic permeability and MI response

Figures 6(i) and 6(ii) show the magnetic permeability (μ') as a function of frequency for as-quenched and heat-treated ***FIN-1*** and ***FIN-2*** ribbons, respectively. It can be observed that the permeability remains almost constant up to a particular frequency and then decreases drastically for all samples. At low frequency (within flat region), the permeability increases with heat-treatment temperature (T_a) up to 575 °C for ***FIN-1*** and 600 °C for ***FIN-2*** and then again decreases on further increasing T_a. This increase in μ' indicates the improvement of magnetic softness in the heat-treated ribbons, which can be attributed to the nucleation and nanocrystallization of soft magnetic Fe_3Si phase. These observations are in good agreement with the obtained coercivity results. Further, the ***FIN-2*** ribbon shows relatively large permeability in their nanocrystalline state than ***FIN-1*** ribbons.

As discussed earlier, the origin of MI is related to the skin effect characterized by magnetic penetration depth δ_m, which in turn related to permeability and its dependence on applied dc magnetic field. The special domain structure of the soft magnetic samples and different magnetization processes, domain-wall motion, and moment rotation cause the change in the transverse magnetic permeability (μ_t') upon application of an external longitudinal dc magnetic field (H_{dc}). According to the classical electromagnetism, the impedance ***Z (f, H_{dc})***

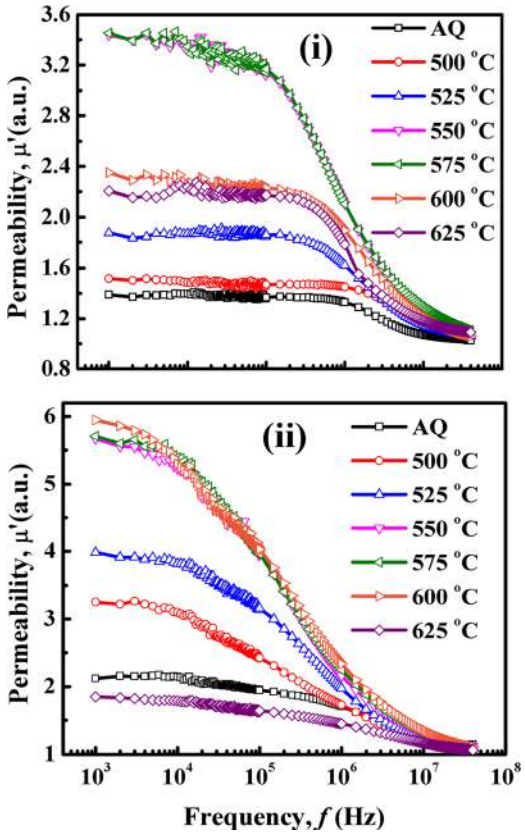

FIG. 6. (Color online) The initial magnetic permeability (μ') spectra of as-quenched and heat-treated ***(i) FIN-1*** and ***(ii) FIN-2*** ribbons.

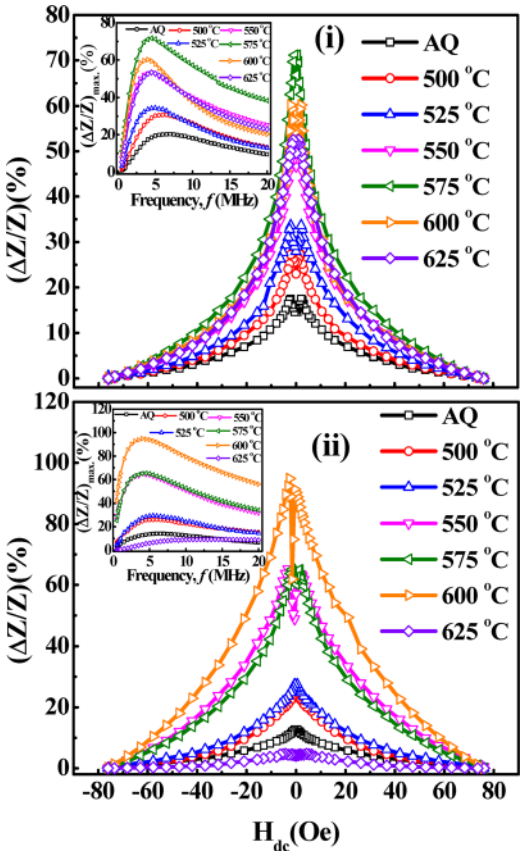

FIG. 7. (Color online) MI profile [i.e., ***(ΔZ/Z)(%)***] measured as a function of external dc magnetic field at frequency, $f = 4$ MHz, for as quenched and heat-treated ***(i) FIN-1*** and ***(ii) FIN-2*** ribbons. ***Inset:*** The frequency dependence of the maximum MI ratio [i.e., $(\Delta Z/Z)_{max}(\%)$] for as-quenched and heat-treated ***(i) FIN-1*** and ***(ii) FIN-2*** ribbons.

changes with the frequency (f) and longitudinal dc magnetic field (H_{dc}) in conjunction with the transverse magnetization. For the simple geometry of a ribbon, Z can be expressed as[17,18]

$$Z = \frac{(1-i)\rho L}{2d\delta_m}$$

$$\delta_m = \left(\frac{\rho}{\pi\mu_t' f}\right)^{1/2}, \qquad (2)$$

where L and d are the length and width of the ribbon, respectively. This formula shows that the behavior of Z is determined by the skin effect. It is worth noting that as the skin effect becomes dominant ($t/\delta_m \gg 1$, where t is the half thickness of the ribbon), the impedance $Z \propto (f\mu_t')^{1/2}$.[7] This is the reason that the best MI response appears only at moderate frequency (1–10 MHz), where the factor $(f\mu_t')^{1/2}$ shows a maximum.

The impedance (Z) as a function of H_{dc} was measured under several frequencies from 0.5–20 MHz. Figs. 7(i) and 7(ii) show the field dependence of MI ratio [i.e., ***(ΔZ/Z)(%)***] at a representative frequency, $f = 4$ MHz for ***FIN-1*** and ***FIN-2***, respectively. It can be observed that the field dependence of ***(ΔZ/Z)(%)*** shows double peak feature for all the ribbons, which increases first with H_{dc} and reaches a maximum $(\Delta Z/Z)_{max}(\%)$ at a critical field and decreases with further increase of H_{dc}. In the present work, the MI profile shows a single peak feature at lower frequencies ($f \leq 1$ MHz), but a double peak feature is observed at higher frequencies ($f > 1$ MHz). In general, there are two types of MI curves, which depend on the effective anisotropy in the sample.[19,20] For a single peak feature, a longitudinal anisotropy with respect to the current and the applied field is essential. The ac magnetization precession occurs under the effect of a transverse ac magnetic field induced by the current. For a two peak feature, a transverse anisotropy with respect to the current and the field is essential. Previous studies have established that the appearance of double peaks is due to transverse anisotropy.[21] At zero applied field, when the magnetization is in the transverse direction, the ac precession under the transverse ac magnetic field is not possible. Applying the dc field and rotating the magnetization away from the transverse direction stimulates the precession and larger ac permeability is established.[22,23] When a small dc magnetic field is applied along the length of the ribbon, the domain-walls move along the length of the ribbon. This happens until the dc field reaches the transverse anisotropy field H_k. Further increment in the dc field could inhibit the wall movement and impel the moment rotation of the domains as the effective permeability decreases sharply leading to a strong MI effect. The two peaks feature confirms the damping of domain-wall motions and shows that tangential magnetization proceeds by the rotation of the moments of the domains.[24] It is observed that the effective anisotropy field lies between 0.5–2.5 Oe at the measuring frequency of 4 MHz and changes to larger value with increasing

frequency for both the ribbons. Since the value of the effective anisotropy field is actually very small in the nanocrystalline samples, the maximum value of MI is observed at nearly zero field ($H_{dc} \sim 0$) for low frequencies ($f \leq 1$ MHz).[25] From the inset of the Figs. 7(i) and 7(ii), it can be noted that the largest MI value observed in the 575 °C heat-treated ribbon is about 72% at $f = 4.5$ MHz for ***FIN-1*** and in the 600 °C heat-treated ribbon is about 95% at $f = 4$ MHz for ***FIN-2*** ribbon. The relatively strong MI effect in the ***FIN-2*** rather than the ***FIN-1*** ribbon is attributed to the lower coercivity and resistivity with larger magnetic permeability as well as finer crystallite size of ***FIN-2*** ribbon, which are dominant in the superior soft magnetic properties. When T_a is greater than these temperatures, the MI value decreases to a great deal, which is likely due to increase in the magnetostriction (λ) and coercivity value, and decrease in the volume fraction of amorphous matrix through which the Fe_3Si grains get coupled. These T_a values (i.e., 575 °C for ***FIN-1*** and 600 °C for ***FIN-2***) determine the optimum heat-treatment temperature for these alloys.

In addition, the inset of Figs. 7(i) and 7(ii) shows the frequency dependence of maximum MI ratio [i.e., $(\Delta Z/Z)_{max}(\%)$] for ***FIN-1*** and ***FIN-2***, respectively. It is found that at frequencies below 1 MHz (i.e., the half thickness of the ribbon, $t < \delta_m$), the maximum value of $(\Delta Z/Z)_{max}(\%)$ is relatively low due to the contribution of the induced magnetoinductive voltage to the magnetoimpedance. When 1 MHz $\leq f \leq$ 5 MHz (i.e. $t \approx \delta_m$), the skin effect is dominant, and hence, a higher $(\Delta Z/Z)_{max}(\%)$ is observed. Beyond $f = 5$ MHz, the $(\Delta Z/Z)_{max}(\%)$ decreases with increasing frequency. It is believed that in this frequency region ($f \geq 5$ MHz), the domain-wall motions are strongly damped owing to eddy currents and only moment rotation takes place, hence contributing less to the transverse magnetic permeability, which declines large $(\Delta Z/Z)_{max}(\%)$.[26] Furthermore, it can be seen that with increase in the heat-treatment temperature, the $(\Delta Z/Z)_{max}(\%)$ increases till the optimum T_a value discussed above and the peak position of $(\Delta Z/Z)_{max}(\%)$ ***vs.*** f shifts towards lower frequencies. This can be ascribed to decrease in resistivity values with the T_a, which is helpful in producing the micro-eddy currents. Due to this, damping of domain-wall motion occurs at lower frequencies. Such a behavior with change in ρ values has been reported earlier.[27]

To this end, the frequency dependence of the magnetic field sensitivity (ξ) has been calculated for the as-quenched and heat-treated ***FIN-1*** and ***FIN-2*** ribbons, using the expression[28]

$$\xi = \frac{2\left(\frac{\Delta Z}{Z}\right)_{\max}(\%)}{\Delta H}, \tag{3}$$

where ΔH is the FWHM of the MI response. The results are shown in Fig. 8. It can be noted that the obtained maximum field sensitivities of the MI effect for the ***FIN-1*** ribbon heat-treated at 575 °C and ***FIN-2*** ribbon heat-treated at 600 °C are 8.3%/Oe at 2.5 MHz and 4.7%/Oe at 2 MHz, respectively. Earlier several attempts have been made to maximize the magnetic field sensitivity (ξ) in MI effect by adding different dopants to the primary alloy systems. Zhang *et al.*[29] have

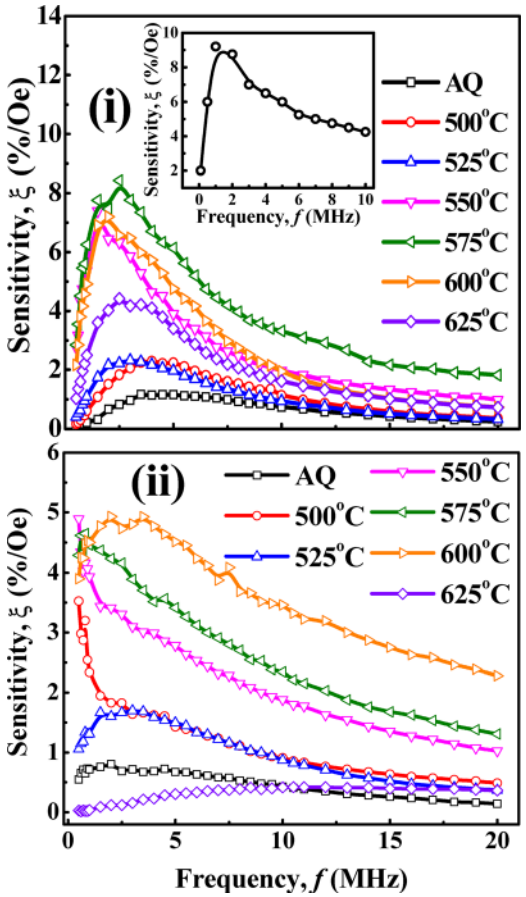

FIG. 8. (Color online) The magnetic field sensitivity (ξ) calculated as a function of frequency for as-quenched and heat-treated ***(i) FIN-1*** and ***(ii) FIN-2*** ribbons. ***Inset: (i)*** Frequency dependence of ξ for 540 °C annealed $Fe_{73}Si_{14}Cu_1Nb_{3.5}B_{8.5}$ ribbons as reported in Ref. 31.

studied amorphous ribbons of $Co_{72-x}Fe_xZr_8B_{20}$ alloys, and decrease of ξ has been found with increase in the Fe concentration. Recently, the values of ξ have been reported for the amorphous and nanocrystalline $(Co_{1-x}Fe_x)_{89}Zr_7B_4$ alloys, and a maximum value of about $\xi = 7$%/Oe at a frequency, $f = 2$ MHz, has been reported for $x = 0$ nanocrystalline alloy.[30] Apart from Co(Fe)-based alloys, Phan *et al.*[31] have investigated the effect of addition of Al to the FeSiCuNbB alloy ribbons. For the nanocrystalline $Fe_{73}Si_{14}Cu_1Nb_{3.5}B_{8.5}$ ribbon, the value of $\xi = 9$%/Oe at $f = 1$ MHz has been reported and these values are further improved with the substitution of Al for Fe in the FeSiCuNbB alloy systems.[26] These reported results are in good agreement with our obtained results. From Fig. 8, it can be noticed that the strong increase of the magnetic field sensitivity (ξ) in the low frequency range ($f \leq 2$ MHz) is likely due to the strong increase of MI which resulted mainly from the domain-wall motion process and to the small FWHM (ΔH) that was almost insensitive to the change of frequency. In the intermediate frequency range (2 MHz $\leq f \leq$ 5 MHz), as the measured frequency range was increased, ΔH increased stronger compared to the increase in MI resulted from both the contributions of domain-wall motion and moment rotation processes, thus, leading to a reduction in ξ, according to the expression (3). At higher frequencies (5 MHz $\leq f$), the strong drop in ξ

resulted from both the decrease in MI and increase in ΔH, with increase in frequency. The field sensitivity of the possible sensor made out of MI material essentially depends on two parameters: (i) the MI ratio and (ii) rate at which the impedance responds to the field. More interestingly, ***FIN-1*** shows relatively larger magnetic response over ***FIN-2*** alloy, in the measured frequency range. The change in FWHM (ΔH) value can be realized from Figs. 7(i) and 7(ii) that the ΔH is more for ***FIN-2*** compared to the ***FIN-1***, though the obtained MI is larger for the ***FIN-2*** ribbon. These results are of practical importance in developing high performance MI sensors.

IV. CONCLUSIONS

We have investigated the influence of nanocrystallization on soft magnetic properties and the MI effect in the $Fe_{73.5}Si_{13.5}Cu_1Nb_3B_9$ (***FIN-1***) and $Fe_{77.2}Si_{11.2}Cu_{0.8}Nb_{3.3}B_{7.5}$ (***FIN-2***) ribbons. With suitable heat-treatment of these amorphous ribbons, one can fine tune the microstructures to generate high performance soft magnetic materials for specific applications. The Fe_3Si phase is identified from X-ray diffraction studies in the nanocrystalline state of the ribbons. Superfine nanocrystalline structure (average grain size of $Fe_3Si \sim 12$ nm) is obtained with controlled heat-treatment of amorphous $Fe_{77.2}Si_{11.2}Cu_{0.8}Nb_{3.3}B_{7.5}$ ribbons. It is shown here that these changes result in improvement of the soft magnetic properties, which are sensitive to the alloy composition. Further, the role played by electrical resistivity and coercivity of the sample in enhancing the MI values has been demonstrated. Though soft magnetic properties and MI values are pronounced in $Fe_{77.2}Si_{11.2}Cu_{0.8}Nb_{3.3}B_{7.5}$ ribbons, higher magnetic response of 8.3%/Oe at 2.5 MHz is obtained for the $Fe_{73.5}Si_{13.5}Cu_1Nb_3B_9$ sample heat-treated at 575 °C. These obtained results can be beneficial for developing high performance MI sensors. The excellent soft magnetic properties play a crucial role in the high MI response. On the other hand, the proper transverse anisotropy with respect to the long dimension of ribbons is also necessary to obtain strong MI effect.

ACKNOWLEDGMENTS

This work is supported by *Defence Research & Development Organization* (Government of India), New Delhi. Authors are also thankful to DST (New Delhi) for nano-initiative and FIST programme for providing the funds for experimental facilities.

[1]M. E. McHenry, M. A. Willard, and D. Laughlin, Prog. Mater. Sci. **44**, 291 (1999).
[2]Y. Yoshizawa, S. Oguma, and K. Yamanchi, J. Appl. Phys. **64**, 6044 (1988).
[3]Y. Yoshizawa, Scr. Mater. **44**, 1321 (2001).
[4]M. Knobel, M. Vazquez, and L. Kraus, "Giant magnetoimpedance," in *Handbook of Magnetic Materials*, edited by K. H. J. Buschow (Elsevier, Amsterdam, 2003), Vol. 15, Chap. V, p. 497.
[5]K. Suzuki, A. Makino, A. Inoue, and T. Masumoto, J. Appl. Phys. **70**, 6232 (1991).
[6]L. V. Panina and K. Mohri, Appl. Phys. Lett. **65**, 1189 (1994).
[7]L. V. Panina, K. Mohri, T. Uchiyama, and M. Noda, IEEE Trans. Magn. **31**, 1249 (1995).
[8]M. Knobel and K. R. Pirota, J. Magn. Magn. Mater. **242**, 33 (2002).
[9]M. Vazquez and A. Hernando, J. Phys. D: Appl. Phys. **29**, 939 (1996).
[10]G. Herzer, J. Magn. Magn. Mater. **294**, 99 (2005).
[11]G. Herzer, in *Encyclopedia of Materials: Science and Technology*, edited by K. H. J. Buschow (Elsevier, Amsterdam, 2008), p. 5897.
[12]M. Tejedor, B. Hernando, M. L. Sanchez, V. M. Prida, J. M. Garcia-Beneytez, M. Vazquez, and G. Herzer, J. Magn. Magn. Mater. **185**, 61 (1998).
[13]B. Majumdar and D. Akhtar, Bull. Mater. Sci. **28**, 395 (2005).
[14]T. Sahoo, A. C. Mishra, V. Srinivas, M. Srinivas, B. Majumdar, and D. Akhtar, J. Magn. Magn. Mater. **321**, 2617 (2009).
[15]K. Zhang, B. Han, L. Xiao, Z. Hua, D. Zhou, T. Zhang, X. Du, B. Yao, X. Xun, and D. Wang, J. Phys. D: Appl. Phys. **40**, 6507 (2007).
[16]J. He, H. Q. Guo, B. G. Shen, K. Y. He, and J. F. Hu, J. Phys.: Condens. Matter **11**, 4251 (1999).
[17]J. D. Jackson, *Classical Electrodynamics* (John Wiley & Sons, New York, 1975).
[18]F. L. A. Machado and S. M. Rezende, J. Appl. Phys. **79**, 6558 (1996).
[19]C. Chen, K. Z. Luan, Y. H. Liu, L. M. Mei, H. Q. Guo, B. G. Shen, and J. G. Zhao, Phys. Rev. B **54**, 6092 (1996).
[20]M. Knobel, M. L. Sanchez, P. Marin, C. Gomez-Polo, M. Vazquez, and A. Hernando, IEEE Trans. Magn. **31**, 4009 (1995).
[21]M. H. Phan and H. X. Peng, Prog. Mater. Sci. **53**, 323 (2008).
[22]D. P. Makhnovskiy, N. Fry, L. V. Panina, and D. J. Mapps, J. Appl. Phys. **96**, 2150 (2004).
[23]D. P. Makhnovskiy, L. V. Panina, and D. J. Mapps, Phys. Rev. B **63**, 144424 (2001).
[24]H. Chiriac, T. A. Ovari, and C. S. Marinescu, IEEE Trans. Magn. **33**, 3352 (1997).
[25]H. Q. Guo, H. Kronmuller, T. Dragon, Z. H. Cheng, and B. G. Shen, J. Appl. Phys. **89**, 514 (2001).
[26]M. H. Phan, H. X. Peng, S. C. Yu, and M. Vazquez, J. Appl. Phys. **99**, 08C505 (2006).
[27]W. Ku, F. Ge, and J. Zhu, J. Phys. D: Appl. Phys. **30**, 1842 (1997).
[28]B. Hernando, M. L. Sanchez, V. M. Prida, M. Tejedor, and M. Vazquez, J. Appl. Phys. **90**, 4783 (2001).
[29]K. Zhang, Z. Lv, Y. Liu, B. Yao, T. Zhang, B. Li, D. Zhou, B. Han, D. Wang, and M. Zeng, J. Phys. D: Appl. Phys. **39**, 4299 (2006).
[30]A. Chaturvedi, N. Laurita, A. Leary, M. H. Phan, M. E. McHenry, and H. Srikanth, J. Appl. Phys. **109**, 07B508 (2011).
[31]M. H. Phan, H. X. Peng, M. R. Wisnom, and S. C. Yu, J. Appl. Phys. **98**, 014316 (2005).